



PS-DeVCEM: Pathology-sensitive deep learning model for video capsule endoscopy based on weakly labeled data

Ahmed Mohammed^{a,**}, Ivar Farup^a, Marius Pedersen^a, Sule Yildirim^b, Øistein Hovde^c

^aDepartment of Computer Science, Norwegian University of Science and Technology, Gjøvik, Norway

^bDepartment of Information Security and Communication Technology, Norwegian University of Science and Technology, Gjøvik, Norway

^cDepartment of gastroenterology, Innlandet Hospital Trust, Gjøvik and Institute of Clinical Medicine, University of Oslo.

ABSTRACT

We propose a novel pathology-sensitive deep learning model (PS-DeVCEM) for frame-level anomaly detection and multi-label classification of different colon diseases in video capsule endoscopy (VCE) data. Our proposed model is capable of coping with the key challenge of colon apparent heterogeneity caused by several types of diseases. Our model is driven by attention-based deep multiple instance learning and is trained end-to-end on weakly labeled data using video labels instead of detailed frame-by-frame annotation. This makes it a cost-effective approach for the analysis of large capsule video endoscopy repositories. Other advantages of our proposed model include its capability to localize gastrointestinal anomalies in the temporal domain within the video frames, and its generality, in the sense that abnormal frame detection is based on automatically derived image features. The spatial and temporal features are obtained through ResNet50 and residual Long short-term memory (residual LSTM) blocks, respectively. Additionally, the learned temporal attention module provides the importance of each frame to the final label prediction. Moreover, we developed a self-supervision method to maximize the distance between classes of pathologies. We demonstrate through qualitative and quantitative experiments that our proposed weakly supervised learning model gives a superior precision and F1-score reaching, 61.6% and 55.1%, as compared to three state-of-the-art video analysis methods respectively. We also show our model's ability to temporally localize frames with pathologies, without frame annotation information during training. Furthermore, we collected and annotated the first and largest VCE dataset with only video labels. The dataset contains 455 short video segments with 28,304 frames and 14 classes of colorectal diseases and artifacts. Dataset and code supporting this publication will be made available on our home page.

© 2022 Elsevier Ltd. All rights reserved.

1. Introduction

There are several colorectal diseases and abnormalities that interfere with the normal working of the colon. Colorectal diseases include colorectal cancer, polyps, ulcerative colitis, diverticulitis etc. Screening and detection of colorectal diseases at an early stage could improve disease management and diag-

nosis. Colonoscopy is considered a gold standard as a screening procedure for colorectal diseases. However, colonoscopy has some limitations including invasiveness, discomfort, and embarrassment for the patient and relatively high cost. These inconveniences may limit the utility of colonoscopy, especially in screening strategies where acceptance of the test is of the utmost importance (Schoofs et al. (2006)). VCE is an alternative to visualize the colon. VCE was first introduced in 2006 as a wireless, minimally invasive technique for the imaging of

^{**}Corresponding author: Tel.: +47-486-766-16

e-mail: mohammed.kedir@ntnu.no (Ahmed Mohammed)

the large bowel that does not require sedation or gas insufflation (Shi et al. (2015)). A single VCE procedure produces approximately 50,000 images and takes 45-90 minutes to review. Therefore, a machine learning system can be used to complement gastroenterologists for fast and accurate diagnosis (Li et al. (2011)).

The detection and classification of colorectal diseases is a very challenging problem due to apparent colon heterogeneity. In fact, colon data contains a high degree of apparent heterogeneity due to varying levels of unpredictable responses caused by the nature of diseases. Moreover, the morphological clues in local neighborhoods of colon images are not consistent across different patients. This makes it difficult to develop an automated disease detection model based on image analysis techniques. A number of image processing based methods have addressed colorectal pathology detection problems in literature (Mohammed et al. (2018b); Bernal et al. (2017); Tajbakhsh et al. (2015); Ronneberger et al. (2015)). These methods do not consider long-term temporal dependencies between frames to improve the performance of detection algorithms. Moreover, they rely on the assumption that pixel-level or frame-level annotation data is available and is trained in a fully supervised manner. However, this assumption is very limiting in a clinical setting as it is expert-intensive and time-consuming to obtain a precise annotation of the pathologies per image. In addition, from a clinical application perspective, a gastroenterologist is required to check for various types of pathologies during a single examination and computer-aided diagnostic techniques are expected to detect as many diseases as possible to circumvent miss-diagnosis. However, the number of pathologies that earlier methods handle is limited to classes of diseases such as polyps (Bernal et al. (2017)) and angiodysplasia (Shvets et al. (2018)). Moreover, the dataset used in training such models lacks class variety to be used in clinical application.

To address these challenges, we propose PS-DeVCEM, a new weakly supervised learning approach for learning frame-level multi-label classification from a given video label. Our model explores robust deep residual features that are invari-

ant to apparent heterogeneity in colon data. We also explore residual LSTM units to take into account the long term photometric and appearance variability. Our approach is based on an objective function that minimizes within-video similarities between positive and negative feature frames, while at the same time learning video-level prediction and contribution from each frame. The proposed method requires only video labels which can easily be obtained from VCE data reader software tags such as RAPID reader (GivenImaging) as a normal working procedure. We formulate the aggregation of positive and negative frame labels using the Bernoulli distribution. The network is trained by optimizing the sum of log-likelihood and cross-entropy for the video prediction. The final video prediction is computed by taking the learned weighted mean of each frame feature embeddings. The learned weights are given by a two-layered neural network that corresponds to the attention. High attention weights indicate key-frames for the detected pathology class and low attention weights show non-informative frames. We exploit the ordering of the attention weights to minimize the similarities between high and low attention frames by training a two-layered neural network which acts as a self-supervision method. The flow diagram of our proposed PS-DeVCEM model is shown in Fig. (1).

Moreover, we assume the video is permutation-variant and modeled with residual bi-directional LSTM. Furthermore, we collect short VCE video segments. The goals are two-fold; to provide a research and development resource for VCE pathology detection, and to provide a way to benchmark and compare different approaches. The dataset contains a total of 28,304 video frames containing 14 classes of diseases and artifacts (bubble and debris) from 40 patients.

The primary contributions of this paper are:

- A self-supervision method to minimize the similarity between positive and negative frames within a video segment. This has an advantage by forcing the attention network to be discriminative between positive and negative instances.
- An end-to-end trainable network that takes video as an

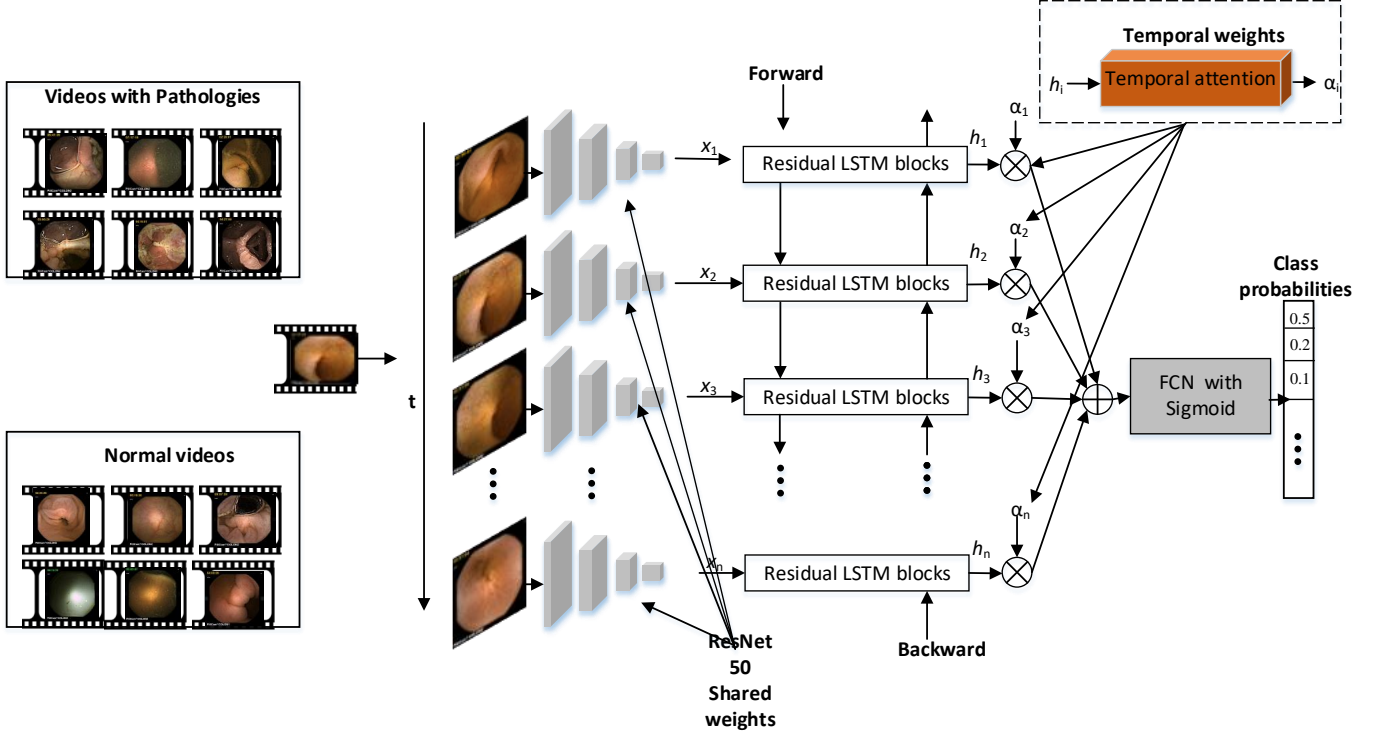


Fig. 1: PS-DeVCEM: The frame features are extracted with ResNet50 network (He et al. (2016)) pre-trained on ImageNet (Deng et al. (2009)). The feature embedding is computed by passing through a residual LSTM block. Finally, the embeddings are aggregated with learned weights. The output of the network is video-level class probabilities for each pathology. For details please refer to Sec. 3.

input and detects key-frames with video-level prediction. The features from each frame in the video are aggregated using learned weights for final video prediction. In addition, we assume temporal dependency between neighboring frames, which is modeled using residual bidirectional long short-term memory blocks.

- A new VCE dataset suited for weakly supervised learning problems. The dataset contains 455 short video segments extracted using RAPID reader software (GivenImaging). There are 28,304 frames with a total of 14 classes of diseases from 40 patients.
- Detailed comparison of existing weakly supervised learning algorithms (Ray and Craven (2005); Andrews et al. (2003); Zhou and Xu (2007); Bunescu and Mooney (2007); Ilse et al. (2018); Paul et al. (2018); Nguyen et al. (2018)) on VCE dataset. We employ a random 50-50 train/test split under the condition that at least each pathology exists in the train/test set.

- Qualitative and quantitative experiments on VCE dataset and comparison with state-of-the-art works show that our proposed method outperforms in-terms of precision and F1-score reaching 61.6% and 55.1% respectively.

We organize the rest of the paper as follows. Section 2 briefly reviews previous works on video analysis and multiple instance learning (MIL). In Section 3 we present the PS-DeVCEM along with the self-supervising method. In Section 4 we present the dataset and comparison of different MIL methods and benchmarks will be discussed. In addition, we present experiments with a different configuration of the proposed method. Finally, in Section 5 we conclude the paper with future direction and discussion.

2. Related Work

In general, there are two approaches in modeling video data context: short and long context modeling. In these methods, the long and short-range dependencies can be well memorized by

sequentially running the network over individual frames. However, designing an architecture for video analysis is a challenging task as it involves computationally expensive tasks such as temporal information fusion strategy, frame feature representation (as compared to end-to-end training) and spatio-temporal feature fusion. The basic building blocks for video analysis with deep learning includes spatial feature extraction unit such as ResNet (He et al. (2016)), VGG (Simonyan and Zisserman (2014)), etc. and temporal feature extraction unit such as optical flow and LSTM (Graves (2013)) units. LSTM (Graves (2013)) is combined with CNN for activity recognition in Long-term recurrent convolutional networks for visual recognition and description (Donahue et al. (2015)). Other alternative approaches extract spatio-temporal features together using 3D convolutions such as C3D (Tran et al. (2015)). Spatio-temporal features such as C3D are used in (Sultani et al. (2018)) for anomaly detection in natural videos. Most of the current state of the art methods use two-stream networks such as ActionVLAD (Girdhar et al. (2017)) at the expense of high computational complexity. This is usually done by fusing extracted spatial and optical flow features independently.

In many endoscopic pathology detection problems, labels are relatively scarce and expensive to obtain. One such case is in VCE, where annotating pathologies frame by frame is arduous and time consuming for medical doctors. Therefore, weakly supervised approaches such as MIL (Maron and Lozano-Pérez (1998); Møllersen et al. (2018)) or fully unsupervised methods of detection and segmentation are required to address the above issue. MIL is a type of weakly supervised learning problem where only group-level, also known as bag level annotation, is available. The instances within the bag are not labeled. For example, the annotation could be a general statement about the category of the pathology in the video without information about the location within the video or frame labels. In the MIL problem formulation (Ilse et al. (2018)), it is assumed that positive bag videos contain at least one instance of a given pathology while a negative bag video depicts none.

MIL algorithms can be divided into two categories, depend-

ing on if the data is an independent samples (images) or temporal based (video).

Independent samples (images): Assumes the data within a positive or negative bag is an independent sample. The simplest approach to MIL is single-instance learning (SIL) (Ray and Craven (2005)) which assigns each instance the label of its bag, creating a supervised learning problem, but mislabeling negative instances in positive bags (Doran and Ray (2014)). In (Andrews et al. (2003)), the standard support vector machine (SVM) formulation (Suykens and Vandewalle (1999)) is modified so that the constraints on instance labels correspond to the fact that at least one instance in each bag is positive (Doran and Ray (2014)). Similarly, in (Bunescu and Mooney (2007)), SVM formulation is modified assuming there are very few positive instances of the positive bags. Other unsupervised methods to MIL include MissSVM (Zhou and Xu (2007)). More recently, Ilse et al. (Ilse et al. (2018)) proposed a permutation-invariant aggregation operator that corresponds to the attention method. Compared to soft attention method as in (Xu et al. (2015)), the aggregation operator is different in that the former is calculated as a dot product while the latter is computed using a two-layered neural network. Moreover, the aggregation operator outperforms commonly used MIL pooling operators (Ilse et al. (2018)). In comparison to other works in endoscopy, (Wang et al. (2016)) addresses endoscopic images with MIL formulation. Wang et al. (Wang et al. (2016)) proposed using endoscopic images with weak labels mined from the diagnostic text. If the diagnostic text does not match any of predefined key words such as Gastric Cancer, Esophageal Cancer, and Esophagitis, the corresponding label of the endoscopic image folder is annotated as negative; otherwise, the label of the endoscopic image folder is annotated as positive. Each frame is considered as independent.

Temporal based (video) MIL: Kotzias et al. (Kotzias et al. (2015)), proposed using group-level labels to learn instance-level classification models. The group-level prediction is given by taking the average of the instances. An objective function is introduced to encourage smoothness of inferred instance-

level labels based on instance-level similarity, while at the same time respecting group-level label constraints. Unlike Kotzias et al. (Kotzias et al. (2015)), MI-Net (Wang et al. (2018)) does not rely on inferring instance-level probabilities. Both of the above approaches are based on neural networks, but Mi-Net is an embedded space aggregation method that uses the MIL pooling layer to focus on learning bag representation. MIL pooling (Pinheiro and Collobert (2015)) layer is used to aggregate instance features into one bag representation. Finally, a fully connected (FCN) layer with sigmoid is used to predict the bag labels. In Paul et al. (2018), spatial and temporal features are extracted using a two-stream network (RGB streams and optical flow) and co-activity similarity loss is proposed to maximize the distance between multiple activities. In (Nguyen et al. (2018)) they consider the problem of untrimmed videos by extracting segment features and sparsity loss on the attention weights for aggregating the segment features.

In general, image-based MIL approaches do not provide temporal localization for the detected pathology and are not suitable for VCE video analysis. In VCE or medical imaging applications in general, experts are interested to know frame-level pathology prediction of the detection algorithm. Compared to (Wang et al. (2016)) endoscopic images are very different from VCE images. VCE images do not have as good image quality as the traditional endoscopy because of high compression and low image resolution due to volume and power limitation. Bad imaging conditions such as low illumination, uncontrolled capsule motion, and peristalsis, will further reduce the qualities of VCE images. Among the temporal and independent sample MIL formulation, none of the above methods exploit the positive and negative segments within a single bag to maximize the distance between the classes. In the proposed method, we show that by using within bag similarity as self-supervision, we can boost the performance of frame localization and VCE video classification.

3. Pathology-sensitive deep learning model

Our aim is to design a weakly supervised model for the purpose of multi-label pathology detection. The model consists of fundamental CNN pipelines, attention, residual LSTM, and self-supervision submodule, as the Fig. (1) shows. The advantage of our attention mechanisms is that it can identify suspected frames and provides a robust video feature representation, while likewise suppressing the irrelevant and non-informative video frames from other classes. Hence, it is very applicable to weakly supervise learning. The residual LSTM submodule is able to focus on temporal features among a long sequence of video frames, and while filter out irrelevant features for representation. Besides, we propose a novel self-supervision mechanism which is used for robust frame localization, because of the apparent colon heterogeneity of the weakly labeled video is quite difficult to distinguish.

We begin by formally defining MIL, and establishing the notation that will be used in the rest of this paper. Let $V = \{f_1, f_2, f_3, \dots, f_N\}$ be a video containing frames $f_1, f_2, f_3, \dots, f_N$ and N is the number of frames in the video. We assume individual labels are available for each video V and is given by G with unknown frame label $\mathbf{y} = \{y_1, y_2, y_3, \dots, y_N\}$. Earlier works in MIL assume binary classification where $y_n \in \{0, 1\}$ (Ilse et al. (2018)), (Wang et al. (2018)). But here we assume a general multi-label classification problem where y_n can assume a set of all possible classes k , $P = \{p_1, p_2, p_3, \dots, p_k\}$ in a multi-label learning problem. P_k is defined as k^{th} abnormality in the dataset and a given video could be labeled to contain multiple abnormalities such as $P = \{\text{"polyp"}, \text{"bleeding"}, \text{"erosion"}\}$. Hence the ground truth dataset has the form $\mathcal{D} = \{(V_1, Y_1), \dots, (V_n, Y_n)\}$ where $V_i \in \mathcal{V}$ and $Y_i \subseteq P$. Using the above notation, the MIL constraints could be represented as:

$$Y = \begin{cases} \mathbf{p} & \text{if } \exists n \text{ s.t. } y_n = \mathbf{p}, \mathbf{p} \subseteq P, n \in N \\ 0, & \text{otherwise} \end{cases} \quad (1)$$

where Y is the predicted video label. Alternative MIL constraint formulation can be given as the maximum class probability over

the frames as:

$$Y = \max_n \{y_n\} \mid y_n = \mathbf{p}, \mathbf{p} \subseteq P, n \in N \quad (2)$$

It is important to note that the frame-level labels, y_n are not available during the training phase and only the video label G is provided. Therefore, our goal is to infer video label Y and frame label y_n by propagating information from video-level to frame-level with a neural network. The motivation for using neural networks is that it is easier to train in an end-to-end fashion. Moreover, previous works (Ilse et al. (2018); Wang et al. (2018); Kotzias et al. (2015); Wu et al. (2015)) have shown that neural network-based MIL approach gives promising results compared to classical approaches (Andrews et al. (2003); Ray and Craven (2005)).

3.1. Residual LSTM

There are three different approaches to come up with a video-level feature representation. These are instance aggregation approach (Andrews et al. (2003)), group aggregation approach (Cheplygina et al. (2015)) and embedded space aggregation approach (Ilse et al. (2018)). The approaches differ in whether they estimate frame-level probabilities or aggregate the embeddings. Instance aggregation approach works by combining instance-level predictions while group-level aggregation approaches use group similarity for clustering positive and negative samples. Embedded space aggregation approaches merge instant features and learn group-level classifier (Wang et al. (2018)). In VCE or medical imaging applications in general, experts are interested to know frame-level pathology prediction of detection algorithm more than video label-level predictions. Hence, instance aggregation approaches are suitable for a medical application. This is because frame-level predictions are paramount as it gives interpretation and explanation for the video prediction. Our approach is based on an aggregation of embeddings with learned aggregation weight, i.e. attention, which gives frame-level inference to the final video prediction. The framework (illustrated in Fig. 1) consists of N fully convolution encoder networks which extract features $x_i = \Phi_\theta(f_i)$, for each frame. The encoder network Φ_θ is ResNet50 (He

et al. (2016)) that is pre-trained on ImageNet (Deng et al. (2009)). However, it is possible to use other networks such as VGG (Simonyan and Zisserman (2014)), DenseNet (Huang et al. (2017)) or similar architectures. Temporal dependency between each frame is modeled using residual LSTM blocks as shown in Fig. 2. The residual LSTM blocks consist of bi-directional LSTMs composed of two LSTM units that leverage the residual connection (Graves and Schmidhuber (2005); Hochreiter and Schmidhuber (1997)). The main idea for using residual connection is to make training easier and avoid performance degradation in deeper networks (He et al. (2016)). The biggest advantage of bi-directional LSTM networks lies in their capability of preserving information over time by the recurrent method.

3.2. Temporal attention

Attention has been shown to improve performance of recurrent neural networks in language translation (Vaswani et al. (2017)) and activity recognition (Sharma et al. (2015)) tasks. Attention is mainly used for easier modeling of long-term dependencies. However, the application of attention to MIL is mainly to model MIL pooling and has been limited (Ilse et al. (2018)). Inspired by (Ilse et al. (2018)), the temporal attention is parameterized using a two layered neural network. The attention block is shown in Fig. (3). However, as shown in Fig. (1) the attention block is trained on residual temporal features rather than frame feature x_i as in (Ilse et al. (2018); Raffel and Ellis (2015)).

The MIL pooling operator aggregates activations of feature maps h_i of the residual block. Let $H = \{h_1, h_2, h_3, \dots, h_N\}$ be frame representation of the residual block. Hence, the MIL pooling layer is given by (Ilse et al. (2018)):

$$Z = \sum_{n=1}^N \alpha_n h_n \quad (3)$$

where

$$\alpha_n = \frac{\exp\{\mathbf{w}^T \tanh(\mathbf{V} \mathbf{h}_n^T)\}}{\sum_{i=1}^N \exp\{\mathbf{w}^T \tanh(\mathbf{V} \mathbf{h}_i^T)\}} \quad (4)$$

where $\mathbf{w} \in \mathbb{R}^{L \times 1}$ and $\mathbf{V} \in \mathbb{R}^{L \times M}$ are parameters of two-layered neural network. Such formulation allows the gradient of cost

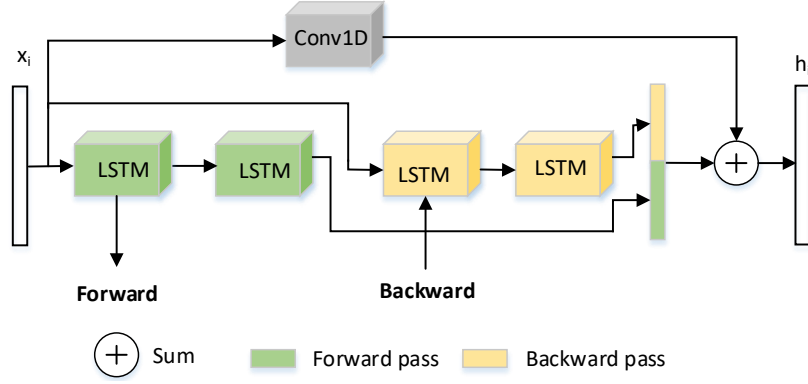


Fig. 2: Residual LSTM block. The input to the residual LSTM blocks are spatial features extracted using cascade of convolutions. The forward and backward LSTM temporal informations are concatenated which represents the temporal feature. The temporal features are summed together with spatial input features x_i , after passing through a 1×1 convolution to have the same feature dimension with temporal features.

function to be back-propagated efficiently as 'tanh' supports both positive and negative values. In this formulation, attention can be seen as producing relative informativeness of the input feature by computing an adaptive weighted average of the residual features.

3.3. Self-supervision

Several recent papers have explored the usage of the temporal ordering of images (Wei et al. (2018); Basha et al. (2012)). Using self-supervised training, temporal ordering has been used for representation learning (Wei et al. (2018)). Inspired by temporal ordering, in this work we propose attention ordering for faster convergence and MIL training regularizer. Our aim is to model how frames with large and small value of attention $\alpha_i \in \alpha$ vary in embedding space $h_i \in \mathbf{H}$. Formally, our method of self-supervision works by enforcing the fact that high valued attention α_i aggregated embeddings h_i should be different from low-valued attention α_i aggregated embeddings. The self-supervision block is shown in Fig. (4). Given frame attention, α , the video frames are clustered into positive and negative bags based on the value of α as shown in Eq.(5) and (6).

$$Z_{bag}^+ = \sum_{b=1}^{B^+ = |\alpha > \frac{1}{N}|} h_b^+ \mid h_b^+ \subseteq \mathbf{h}, \alpha_b > \frac{1}{N} \quad (5)$$

$$Z_{bag}^- = \sum_{b=1}^{B^- = |\alpha \leq \frac{1}{N}|} h_b^- \mid h_b^- \subseteq \mathbf{h}, \alpha_b \leq \frac{1}{N} \quad (6)$$

where B^+ and B^- are the cardinalities of the set $\alpha > \frac{1}{N}$ and $\alpha \leq \frac{1}{N}$ respectively.

Finally, positive and negative bag feature embeddings, Z_{bag}^+, Z_{bag}^- , are used for training a two-layered neural network. The network is trained with the ground truth value of "1" if the bags are the same and "0" otherwise. In other words, the proposed self-supervision acts as a regularizer by maximizing the distance between positive and negative bags in embedding space.

3.4. Loss function

The inputs of our model consist of a sequence of video frames and their corresponding pathology label (ground truth). Considering we would like to learn both temporal attention and video-level predictions, we formulated the loss function shown in Eq. (7). The purpose of the training process is to minimize such loss function \mathcal{L} , where M is the size of the training set, g are the ground truth labels, and y are the predicted probabilities.

$$\mathcal{L} = \frac{1}{M} \sum_{m=1}^M g_m \log(y_m) + \frac{\lambda}{M} \sum_{m=1}^M g_m^{bag} \log(y_m^{bag}) - (1 - g_m^{bag}) \log(1 - y_m^{bag}) \quad (7)$$

The first term part of Eq. (7) minimizes video-level prediction loss. Note that unlike (Sharma et al. (2015); Xu et al. (2015)), here the attention is learned implicitly without any constraint in the loss function. The second part of the equation represents

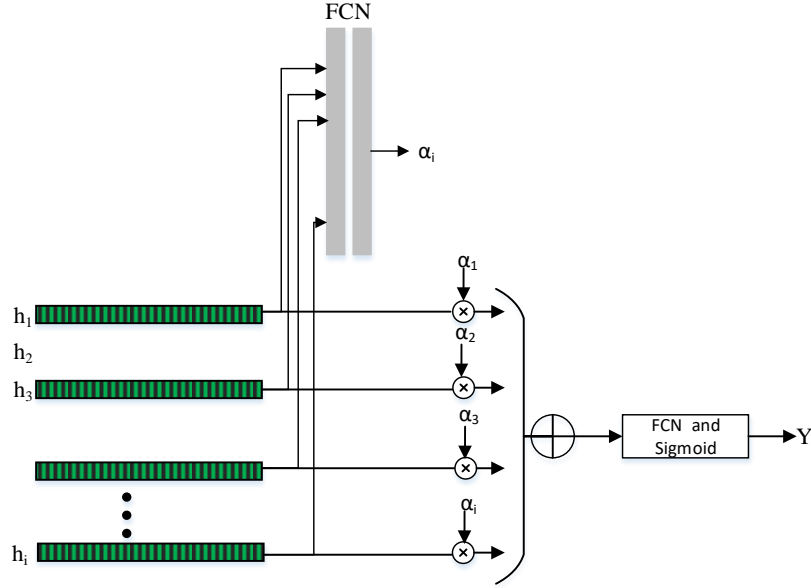


Fig. 3: Temporal attention: Given the spatial and temporal feature as input from our residual LSTM block, the temporal attention block computes the relevance of each frame for the final video feature representation. Once the attention values α_i for each frame is computed, the summed weighted features are passed through a fully connected network for video level prediction.

self-supervision loss which is a negative log-likelihood based on the Bernoulli distribution. g_m^{bag} is the ground truth label, which is “1” if the bags are the same or “0” otherwise. y_m^{bag} is the predicted probabilities of the bag.

4. Experiment

In this section, we provide an analysis of our proposed PS-DeVCEM model and evaluate our temporal attention method. Then we compare our model with representative state-of-the-art methods (Ray and Craven (2005); Andrews et al. (2003); Zhou and Xu (2007); Bunescu and Mooney (2007); Ilse et al. (2018); Paul et al. (2018); Nguyen et al. (2018)) and evaluate them quantitatively for each of the pathologies.

4.1. Dataset

This work is joint work with a hospital aimed at medical application. The dataset is collected using PillCam COLON I and II VCE devices from 40 patients. PillCam COLON VCE is 11mm x 31mm in size and it is equipped with two cameras acquiring pictures from both ends of the capsule with an adaptive frame rate of 4-35 frames per second (Mohammed

et al. (2018a)). The dataset consists of 455 short segment videos with a total of 28,304 images. We extracted the video segments using the RAPID reader software (GivenImaging) from the gastroenterologist tagged section of approximately 8-hour video per patient as shown in Fig. (5). Each training sample consists of 50 to 100 frames with the middle frame thumb-nailed by a gastroenterologist. The videos are of 512×512 resolution. The dataset is labeled by a single doctor and later on verified by a second medical doctor (experienced gastroenterologist). The dataset is unbalanced as some pathologies are more frequent than others. The dataset is representative of a clinical setting and we kept rare pathologies in the dataset. The dataset includes 14 classes showing pathological findings and cleansing quality of the endoscopic procedures, Table 1.

Dataset splitting: For proper ablation study and benchmarking, we split the dataset into two groups, train/test. Data splitting can be formulated as a statistical sampling problem. There are various statistical sampling techniques that could be employed to split the data (May et al. (2010)). In our case, we used simple random sampling with 50% of the data for training and 50% for testing. In such a case, we try to make a train/test

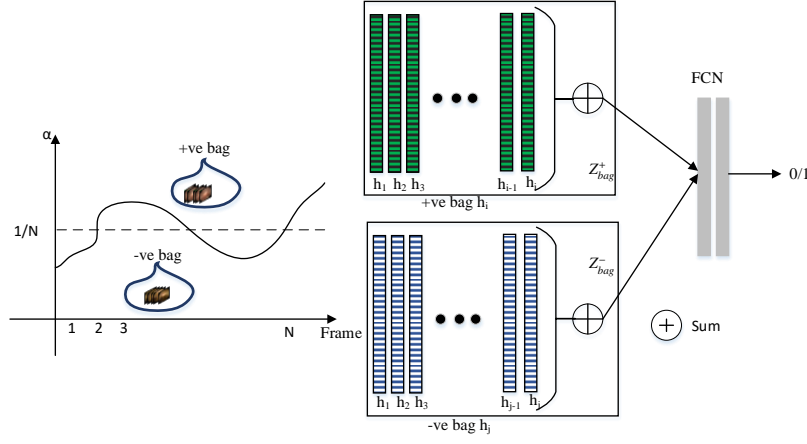


Fig. 4: Self-supervision: Frames with high attention values correspond to key frames. Key frames are more likely to contain a given pathology and similar in appearance within a given video. The positive and negative bags are estimated by clustering the frames based on the attention. The aggregation of positive and negative bag embeddings h_i is used for training the self-supervision network together with multi-label video classification network.

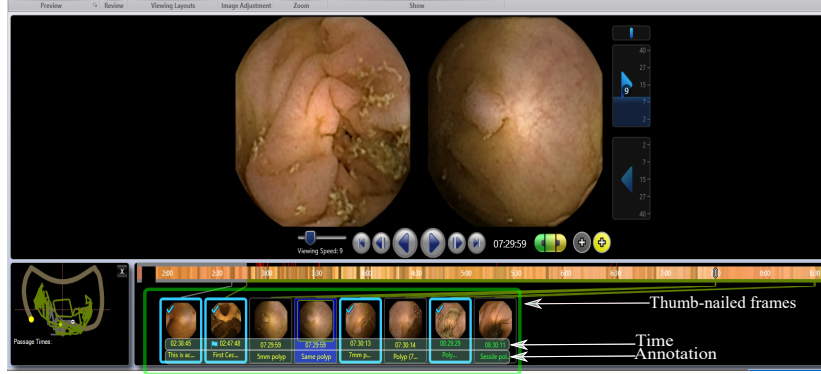


Fig. 5: Annotation: The top right and left images show the rear and front camera view of PillCam COLON II capsule. Gastroenterologist thumb-nail a given instances of a suspected pathology with annotation text as shown above. A video with 50 to 100 frames containing such thumb-nailed frame is extracted as a training and test video.

set to contain a more or less equal number of pathological findings and artifacts. The train/test set video are sampled randomly from all patients to insure the trained model learned to distinguish the diseases rather than different patients. Table 1 outlines information about the pathologies and the number of videos in the training and testing set.

Data augmentation: We randomly flipped the video segments horizontally or vertically and randomly zoom parts of the video segment to prevent the network from overfitting. We acknowledge that extensive data augmentation techniques (for instance, swapping temporal order, perspective distortion) will likely lead to improved performance. However, since the purpose of this evaluation is to benchmark different methods, we rely on

simple data augmentation techniques.

Implementation: Our model is implemented with a Pytorch library with a single NVIDIA TITAN X GPU. The images are resized into fixed dimensions with a spatial size of 224×224 before feeding the encoder networks. The encoder network follows the typical architecture of ResNet50 (He et al. (2016)), which has been widely used as the base network in many vision applications. The encoders are shared and initialized with a pre-trained weight trained on the ImageNet dataset. The last fully-connected layer of the network was truncated and the output of average pooling is used for frame representation. We set the sequence length to 30 frames per video segment with a bi-directional LSTM hidden-state dimension of 1024. Longer

Table 1: Content of PS-DeVCEM dataset: Note that some of the video segments are labeled for multiple pathologies. Each video is labeled by one gastroenterologist and checked by a second gastroenterologist for quality control. On average, the training and test data has 1.74 and 1.85 labels per video respectively. In the training data number of videos having one, two, three, four, and five labels are 107, 88, 16, 14, and 2 videos respectively. In the test data videos having one, two, three, four, five, six labels are 98, 89, 21, 17, 2, and 1 respectively.

Pathology	Erosions	Debris	Diverticulosis	Erythema	Granularity	Haemorrhage	Inflammation	Normal	Oedema	Angioectasia	Polyp	Pseudopolyp	Tumor	Ulceration	Total
# training videos	54	72	17	16	27	17	22	45	5	1	32	28	8	32	227
# testing videos	64	84	16	21	28	20	24	41	7	1	30	29	3	45	228

videos are sampled uniformly to a constant size of 30 frames. For more details, please refer to Appendix.

Frame-level inference: The importance of each frame to the final video level representation is determined by the value of α as shown in Eq. (4). Frames with a high value of α indicate where in the video a given pathology is suspected, hence providing frame-level inference.

Evaluation: We report our experimental results using the PS-DeVCEM dataset. Following earlier works, Tajbakhsh et al. (2015); Bernal et al. (2017), evaluation is done using precision, recall, F1-score, and sensitivity metrics. Low recall could lead to miss-diagnosis while low precision could add extra work to the gastroenterologist. Hence, having a high performance with a balanced Type I and II error and preferably lower Type II error would be desirable. In all of our experiments, we kept the base network to ResNet50 and we examined how our PS-DeVCEM approach handles challenging cases of video and frame-level inference.

Ablation study on temporal attention and self-supervision:

After getting visual feedback from a gastroenterologist on temporal attention accuracy, we performed multiple experiments to improve the accuracy of the attention block. There are various ways to train the temporal attention block based on the input feature used. To analyze the impact of using various input features and the importance of each block in the proposed framework, we carry out extensive ablation studies on the PS-DeVCEM dataset. The results are summarized in Table 2. Table 2 shows multiple experiments on temporal attention block positioning and training the network. We evaluate the optimal placement of temporal attention block as follows.

Learning on frame feature (AttenConv): The temporal attention block is fed with the extracted feature from each frame x_i . The

frame representation and temporal attention are given in Eq. (8) and (9). Each convolution feature is weighted with computed value α_n before feeding into the LSTM network. The final state of the LSTM (h_N) is used for training the neural network. This is equivalent to applying temporal attention to extracted features and model the temporal information with LSTM. Therefore, after temporal attention the extracted feature x_n becomes

$$\hat{x}_n = x_n \alpha_n \quad (8)$$

where

$$\alpha_n = \frac{\exp\{\mathbf{w}^T \tanh(\mathbf{V} \mathbf{x}_k^T)\}}{\sum_{n=1}^N \exp\{\mathbf{w}^T \tanh(\mathbf{V} \mathbf{x}_k^T)\}} \quad (9)$$

Learning on frame feature for LSTM attention (AttenConvLSTM): Another alternative to AttenConv configuration is to train the attention module on the input frame feature while weighting the hidden state of LSTM block with the computed attention weights. Hence, for this configuration, the MIL pooling layer is given by Eq. (3) and the temporal attention weights are calculated with Eq. (9). In other words, each frame contribution to the final video-level representation is determined with extracted feature x_i without any temporal information.

Learning attention on hidden states of LSTM (AttenLSTM): This is a typical approach of computing attention with LSTM blocks for human action recognition (Song et al. (2017); Sharma et al. (2015); Xu et al. (2015)) tasks. In this case, the temporal attention is computed using the hidden state representation of LSTM h_i and extracted feature x_i . The MIL pooling layer is given by Eq. (3) with temporal attention weights as shown in Eq. (4). The difference between this configuration and the proposed method is, in PS-DeVCEM we use the residual block shown in Fig. (2) and self-supervision Fig. (4).

Guided AttenLSTM (GuidedLSTM): In this configuration, we

extended our earlier experiment, AttenLSTM by introducing the self-supervision network that is introduced in Section 3.3. The self-supervision block is trained to minimize the distance between high and low attention weighted frame feature representation. The main purpose of this experiment is to examine the efficacy of self-supervision on the overall accuracy of the method and temporal attention.

Ablation study results: Table 2 lists the results of the four variants of our framework discussed along with the temporal attention weights shown in Fig. (6). From the experiments, we note the following points for improved trainable MIL pooling layer. First, learning attention weights from LSTM hidden state gives a better result compared to convolution features. Although VCE videos are taken with an adaptive frame rate of 4-35 frames per second, temporal information helps in improving the overall performance of the networks. Moreover, as shown in Fig. (6), attention weights are not smooth for visually similar neighboring frames. Secondly, even with temporal information learning attention from convolutional features x_i alone performs worse than learning attention weights with LSTM hidden states. Thirdly, our method with residual features and self-supervision gives a better result with 8.7% and 6.8% improvement in average precision and average recall as compared to second-best metrics for each metric respectively. It is important to note that the above experiments are done under the same experimental setup with different configuration outlined above.

Temporal attention weights are shown in Fig. (6) examine contributions from each frame to the final video contribution. The attention weights give important insight into the location of the pathology in the video. Note that, since the attention weights are normalized, the value corresponds to the probability of each frame to have a given pathology. Although GuidedLSTM performs slightly less than AttenLSTM, the attention weights are narrower as they are more discriminative between positive and negative classes. On the other hand self-supervision with residual blocks and AttenLSTM attends the correct frames as compared to other methods. (i.e. few frames on the left and middle of the video shows polyp)

Comparison with state-of-the-art: In this subsection, we present our experimental results with classical and recent MIL works using the PS-DeVCEM dataset. In order to compare with (Ray and Craven (2005); Bunescu and Mooney (2007); Zhou and Xu (2007)), we extracted image features with ResNet50 architecture for similar representation with other methods. It is important to note that these methods are proposed for binary cases. Therefore, we apply the algorithms for each class of pathologies and solve for binary MIL formulation. We also compare with deep learning-based approaches (Ilse et al. (2018); Paul et al. (2018); Nguyen et al. (2018)). The feature extraction part of (Ilse et al. (2018); Paul et al. (2018); Nguyen et al. (2018)) is replaced with ResNet50 for uniform feature representation. The loss function in (Ilse et al. (2018)) is modified to multi-label classification problem. Table 3 shows that the proposed method does achieve a state-of-the-art result on the PS-DeVCEM dataset. All deep learning-based methods (Ilse et al. (2018); Paul et al. (2018); Nguyen et al. (2018)) are trained end-to-end with ResNet50 as a backbone network for feature extraction. It is important to note that both Nguyen et al. (2018) and Paul et al. (2018) are weakly supervised works that are proposed for activity recognition in a video. For Nguyen et al. (2018) we used a segment size of one and in Paul et al. (2018) we only used the RGB stream. As in Table 3, it is clear that the proposed PS-DeVCEM improves F1-score and precision when using residual LSTM blocks and self-supervision. However, in special cases where pathology exists throughout the video Fig. (8), our proposed method underestimates the frame attention weight (i.e. the video frames are visually similar but the attention values tend to be different). This is due to the dataset imbalance in the training examples for each pathology.

Self-supervision: In order to understand how self-supervision loss affect the detection performance, we have included further experiment in Table 3. As shown in Table 3, self-supervision improves the overall performance of the network by maximizing the distance between positive and negative feature embeddings. The self-supervision allows frames with similar feature to have similar attention weights and regularizes the at-

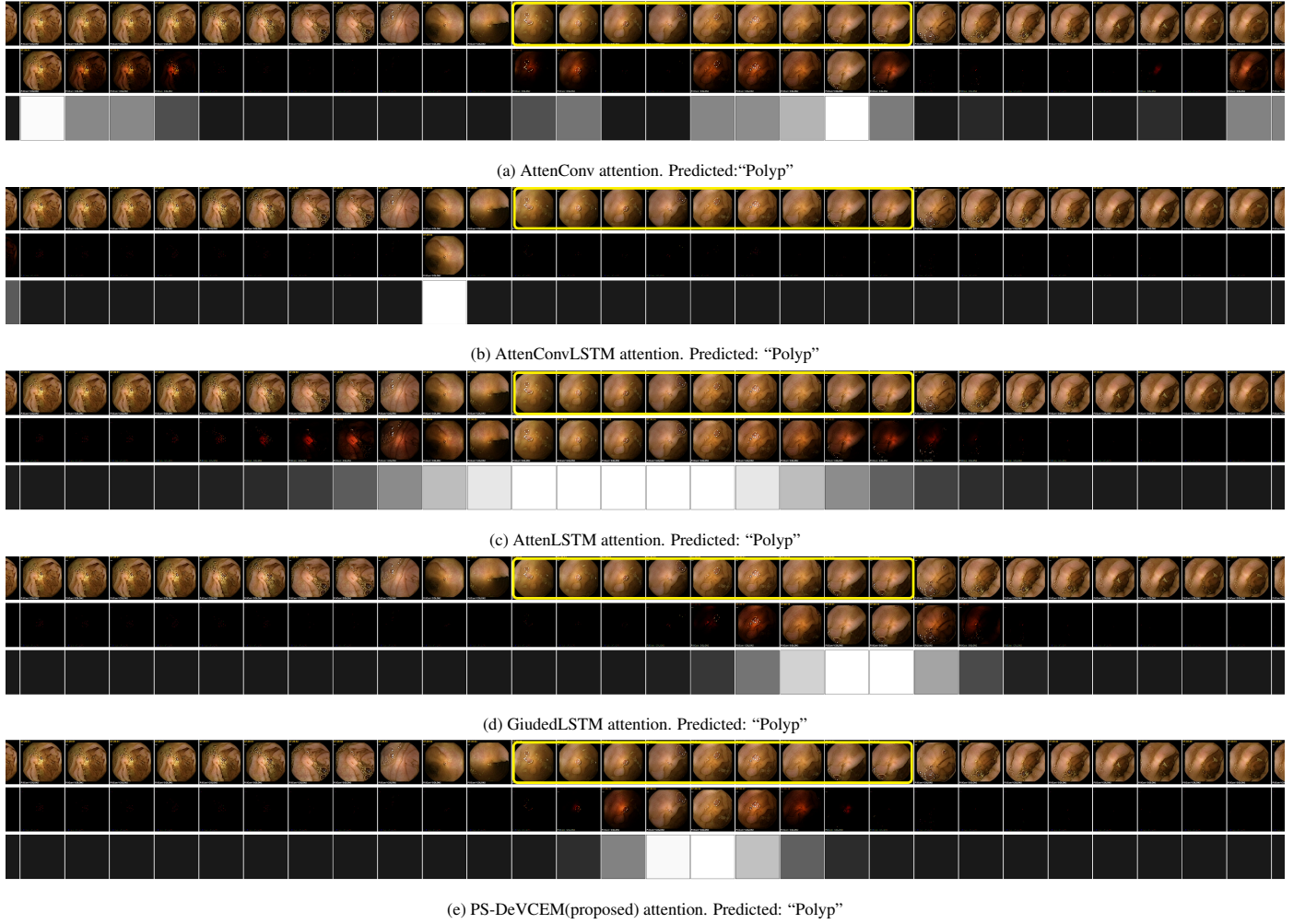


Fig. 6: Example of attention weights for different configurations. The top frames show the sequence of video frames with the corresponding attention in the middle frame. Yellow bounding boxes on the top frames show frame level annotation. The last row shows gray scale coded image with black the irrelevant frames and white the relevant frames. Attention frames vary from Blank (Black) to the original frame corresponding to low and high value of attention weights, respectively. The attention images are encoded as $(I^{0.0001 + \frac{1}{attention}})$. The ground truth label for the video is "Polyps" shown in yellow box, with expected attention to the middle and left side of the video. It can be seen that our proposed method gives smooth attention as well as better localization of suspected frames.(Best viewed in color)

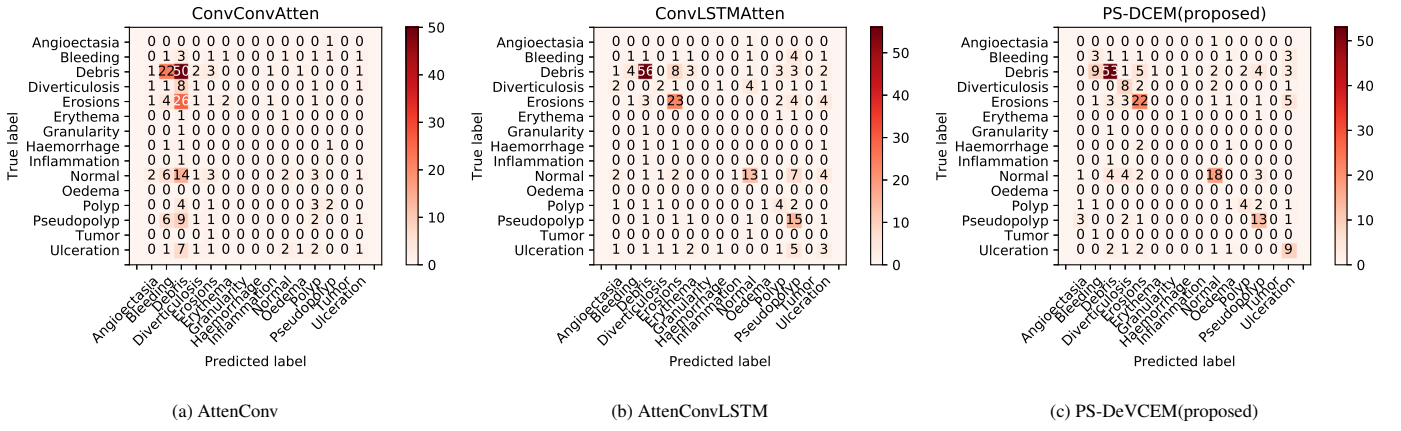


Fig. 7: Learning attention: In Fig. (7a), the video feature is computed by using the weighted sum of features x_i using the attention weights computed based on the convolutional feature while in Fig. (7b) and (7c) is computed using the output of the residual LSTM block. In Fig. (7a), we can see that normal frames are confused for bleeding, debris and diverticulosis as compared to the proposed method. Furthermore, with our proposed self-supervision very similar classes such as ulcerations and erosion are better separated. In the above figure, Fig. (7a) represents independent sample based method while Fig. (7b) and (7c) represent temporal based MIL formulations as discussed in related work section.

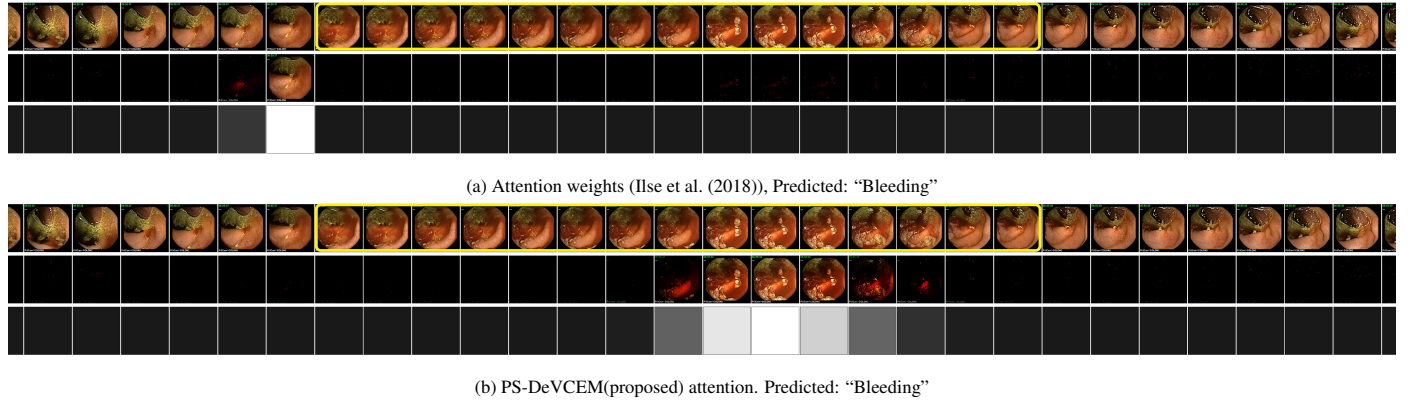


Fig. 8: Comparison of temporal attention weights. The ground truth label for the video is "Bleeding", in most of the frames. In (Ilse et al. (2018)), it is assumed that each instance is permutation-invariant and the attention modules are not able to localize the keyframes. Our approach considers neighboring instances to be similar and therefore gives a smooth and better localization of the keyframes.

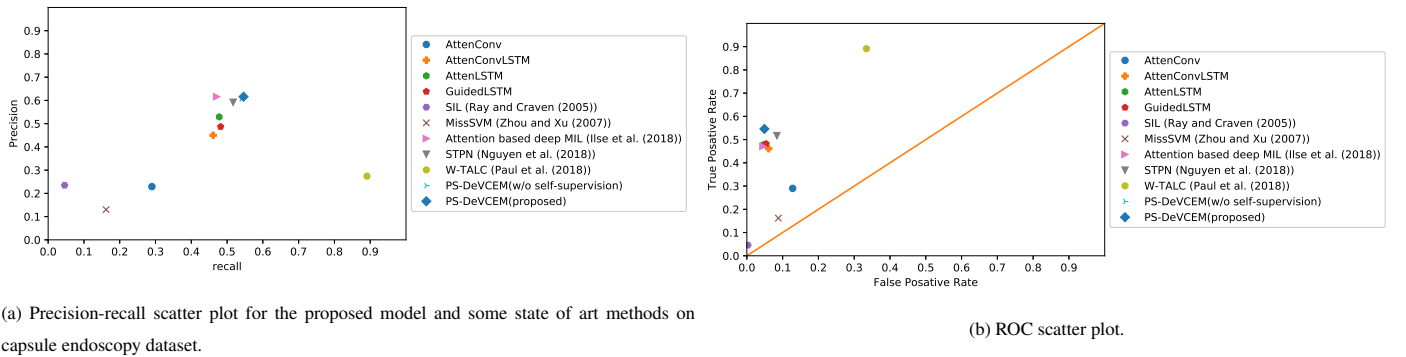


Fig. 9: Performance evaluation on multi-label video classification. The plot shows comparison of state of the art methods with different ways of computing the attention weights. From precision-recall plot, we can see that W-TALC (Paul et al. (2018)) gives a high recall value and small precision score compared to the proposed method. However, low precision score results in additional work for the gastroenterologist as false positive sample videos need to be reviewed.

Table 2: Ablation study result: The values are averaged for all pathologies. The table shows different ways of computing attention weights and its impact on the overall performance of video classifiers. With the proposed residual LSTM block and self-supervision, the final video representation gives better performance.

Method	Precision	Recall	F1-score	Specificity
AttenConv	0.229	0.290	0.246	0.872
AttenConvLSTM	0.450	0.461	0.443	0.939
AttenLSTM	0.529	0.478	0.487	0.954
GuidedLSTM	0.487	0.482	0.458	0.946
PS-DeVCEM(proposed)	0.616	0.546	0.551	0.951

Table 3: Comparison with other MIL algorithms: The values are averaged for all pathologies. Note that STPN (Nguyen et al. (2018)) , W-TALC (Paul et al. (2018)) and Attention based deep MIL (Ilse et al. (2018)) are deep neural network based methods while SIL (Ray and Craven (2005)) and MissSVM (Zhou and Xu (2007)) are based on SVM classifier.

Method	Precision	Recall	F1-score	Specificity
SIL (Ray and Craven (2005))	0.235	0.046	0.066	0.997
MissSVM (Zhou and Xu (2007))	0.130	0.162	0.123	0.912
Attention based deep MIL (Ilse et al. (2018))	0.616	0.471	0.513	0.955
STPN (Nguyen et al. (2018))	0.592	0.517	0.536	0.916
W-TALC (Paul et al. (2018))	0.274	0.891	0.416	0.666
PS-DeVCEM(w/o self-supervision)	0.606	0.54	0.54	0.951
PS-DeVCEM(proposed)	0.616	0.546	0.551	0.951

tention weights to be consistent.

Discussion: By using self-supervision and residual LSTM blocks, we effectively optimized the performance of the proposed approach. By first classifying group of frames into positive and negative classes and further classifying the frames as a whole into separate categories progressively, the self-supervision mechanism improves feature discrimination between similar classes. Compared to metric learning techniques such as Paul et al. (2018) as shown in Table 3, the proposed method relies on a weak supervision to improve positive and negative class feature representations. Alternatively approaches to the self-supervision mechanism including metric learning and siamese network Bromley et al. (1994) variants can be used with the caveat that each video could contain multiple pathologies and some pathologies are more-likely to occur together than others. Furthermore, since such approach give a high self-supervision, dataset imbalance and representation learning need

to be taken into consideration. From the confusion matrix plot in Fig. (7), we can observe that similar classes like debris and erosion, erosion and ulceration are challenging to visually separate. With the proposed weak self-supervision, we are able to improve discriminative feature representation without directly addressing class imbalance problem. However, we note that the frame-level inference could be influenced depending on the following points. Firstly, the dataset is collected with a central part of the video tagged for pathologies. This could influence the learning process in practical settings since it can bias the learning algorithm to memorize the location of the tagged pathology. Secondly, the residual LSTM blocks aggregate information temporally which could miss-align the attention to an incorrect segment of the video. Higher attention weight could be given to frame location where the highest temporal information available. One approach to address the above issues is to collect additional datasets and longer sequences. However, de-

spite being trained in a purely weakly-supervised manner, our approach gives the state-of-the-art result for pathology detection.

As shown in Fig. (9), temporal information aggregation using attention units improves the overall performance of any of methods. However, the method and input to the attention units affect the performance video classification task as well as frame localization. Experimental results as shown in the ablation study indicate that residual LSTM blocks as input to a two layered neural network attention units give a better performance compared to alternative approaches.

5. Conclusion

In this work, we proposed PS-DeVCEM: a pathology-sensitive end-to-end deep model based on weakly labeled capsule endoscopy data. We introduced a self-supervision method and residual LSTM blocks for video and frame-level prediction, further improving the interpretability of the proposed framework. Furthermore, we developed the first VCE dataset with video labels aiming at MIL formulation with a total of 455 short-segment videos. Moreover, experimental results on the PS-DeVCEM database show that the proposed method achieves the best performance on precision and F1-score metrics. Finally, we believe that the PS-DeVCEM dataset and the proposed approach will inspire similar works as the dataset and code will be available with this publication.

As future work, we plan to improve the video frame localization through domain knowledge of the pathologies. Moreover, some pathologies such as inflammations have longer temporal dependencies and handling longer temporal dependencies can further improve the performance. Furthermore, we are planning to diversify our dataset and collect more videos to improve the frame-level localization of pathologies.

References

- Andrews, S., Tschantz, I., Hofmann, T., 2003. Support vector machines for multiple-instance learning, in: *Advances in neural information processing systems*, pp. 577–584.
- Basha, T., Moses, Y., Avidan, S., 2012. Photo sequencing, in: *European Conference on Computer Vision*, Springer. pp. 654–667.
- Bernal, J., Tajkubaksh, N., Sánchez, F.J., Matuszewski, B.J., Chen, H., Yu, L., Angermann, Q., Romain, O., Rustad, B., Balasingham, I., et al., 2017. comparative validation of polyp detection methods in video colonoscopy: results from the miccai 2015 endoscopic vision challenge. *IEEE transactions on medical imaging* 36, 1231–1249.
- Bromley, J., Guyon, I., LeCun, Y., Säckinger, E., Shah, R., 1994. Signature verification using a “siamese” time delay neural network, in: *Advances in neural information processing systems*, pp. 737–744.
- Bunescu, R.C., Mooney, R.J., 2007. Multiple instance learning for sparse positive bags, in: *Proceedings of the 24th international conference on Machine learning*, ACM. pp. 105–112.
- Cheplygina, V., Tax, D.M., Loog, M., 2015. Multiple instance learning with bag dissimilarities. *Pattern Recognition* 48, 264–275.
- Deng, J., Dong, W., Socher, R., Li, L.J., Li, K., Fei-Fei, L., 2009. Imagenet: A large-scale hierarchical image database, in: *2009 IEEE conference on computer vision and pattern recognition*, Ieee. pp. 248–255.
- Donahue, J., Anne Hendricks, L., Guadarrama, S., Rohrbach, M., Venugopalan, S., Saenko, K., Darrell, T., 2015. Long-term recurrent convolutional networks for visual recognition and description. *Proceedings of the IEEE Conference on Computer Vision and Pattern Recognition*, 2625–2634.
- Doran, G., Ray, S., 2014. A theoretical and empirical analysis of support vector machine methods for multiple-instance classification. *Machine Learning* 97, 79–102.
- Girdhar, R., Ramanan, D., Gupta, A., Sivic, J., Russell, B., 2017. Actionvlad: Learning spatio-temporal aggregation for action classification, in: *Proceedings of the IEEE Conference on Computer Vision and Pattern Recognition*, pp. 971–980.
- GivenImaging, . Rapid™ reader software v8.3 update — medtronic. <https://www.medtronic.com/covidien/en-us/support/software/gastrointestinal-products/rapid-reader-software-v8-3.html>. (Accessed on 03/07/2019).
- Graves, A., 2013. Generating sequences with recurrent neural networks. *arXiv preprint arXiv:1308.0850*.
- Graves, A., Schmidhuber, J., 2005. Framewise phoneme classification with bidirectional lstm and other neural network architectures. *Neural Networks* 18, 602–610.
- He, K., Zhang, X., Ren, S., Sun, J., 2016. Deep residual learning for image recognition, in: *Proceedings of the IEEE conference on computer vision and pattern recognition*, pp. 770–778.
- Hochreiter, S., Schmidhuber, J., 1997. Long short-term memory. *Neural computation* 9, 1735–1780.
- Huang, G., Liu, Z., Van Der Maaten, L., Weinberger, K.Q., 2017. Densely connected convolutional networks, in: *Proceedings of the IEEE conference on computer vision and pattern recognition*, pp. 4700–4708.
- Ilse, M., Tomczak, J.M., Welling, M., 2018. Attention-based deep multiple instance learning. *arXiv preprint arXiv:1802.04712*.

- Kotzias, D., Denil, M., De Freitas, N., Smyth, P., 2015. From group to individual labels using deep features, in: *Proceedings of the 21th ACM SIGKDD International Conference on Knowledge Discovery and Data Mining*, ACM. pp. 597–606.
- Li, B., Meng, M.Q.H., Lau, J.Y., 2011. Computer-aided small bowel tumor detection for capsule endoscopy. *Artificial intelligence in medicine* 52, 11–16.
- Maron, O., Lozano-Pérez, T., 1998. A framework for multiple-instance learning, in: *Advances in neural information processing systems*, pp. 570–576.
- May, R.J., Maier, H.R., Dandy, G.C., 2010. Data splitting for artificial neural networks using som-based stratified sampling. *Neural Networks* 23, 283–294.
- Mohammed, A., Farup, I., Yildirim, S., Pedersen, M., Hovde, Ø., 2018a. Variational approach for capsule video frame interpolation. *EURASIP Journal on Image and Video Processing* 2018, 30.
- Mohammed, A., Yildirim, S., Farup, I., Pedersen, M., Hovde, Ø., 2018b. Y-net: A deep convolutional neural network for polyp detection. *British machine vision conference(BMVC)*, arXiv preprint arXiv:1806.01907 .
- Møllersen, K., Hardeberg, J.Y., Godtliebsen, F., 2018. A bag-to-class divergence approach to multiple-instance learning. arXiv preprint arXiv:1803.02782 .
- Nguyen, P., Liu, T., Prasad, G., Han, B., 2018. Weakly supervised action localization by sparse temporal pooling network, in: *Proceedings of the IEEE Conference on Computer Vision and Pattern Recognition*, pp. 6752–6761.
- Paul, S., Roy, S., Roy-Chowdhury, A.K., 2018. W-talc: Weakly-supervised temporal activity localization and classification, in: *Proceedings of the European Conference on Computer Vision (ECCV)*, pp. 563–579.
- Pinheiro, P.O., Collobert, R., 2015. From image-level to pixel-level labeling with convolutional networks, in: *Proceedings of the IEEE Conference on Computer Vision and Pattern Recognition*, pp. 1713–1721.
- Raffel, C., Ellis, D.P., 2015. Feed-forward networks with attention can solve some long-term memory problems. arXiv preprint arXiv:1512.08756 .
- Ray, S., Craven, M., 2005. Supervised versus multiple instance learning: An empirical comparison, in: *Proceedings of the 22nd international conference on Machine learning*, ACM. pp. 697–704.
- Ronneberger, O., Fischer, P., Brox, T., 2015. U-net: Convolutional networks for biomedical image segmentation, in: *International Conference on Medical image computing and computer-assisted intervention*, Springer. pp. 234–241.
- Schoofs, N., Deviere, J., Van Gossum, A., 2006. Pillcam colon capsule endoscopy compared with colonoscopy for colorectal tumor diagnosis: a prospective pilot study. *Endoscopy* 38, 971–977.
- Sharma, S., Kiros, R., Salakhutdinov, R., 2015. Action recognition using visual attention. arXiv preprint arXiv:1511.04119 .
- Shi, H.Y., Ng, S.C., Tsoi, K.K., Wu, J.C., Sung, J.J., Chan, F.K., 2015. The role of capsule endoscopy in assessing mucosal inflammation in ulcerative colitis. *Expert review of gastroenterology & hepatology* 9, 47–54.
- Shvets, A.A., Iglovikov, V.I., Rakhlin, A., Kalinin, A.A., 2018. Angiodysplasia detection and localization using deep convolutional neural networks, in: *2018 17th IEEE International Conference on Machine Learning and Applications (ICMLA)*, IEEE. pp. 612–617.
- Simonyan, K., Zisserman, A., 2014. Very deep convolutional networks for large-scale image recognition. arXiv preprint arXiv:1409.1556 .
- Song, S., Lan, C., Xing, J., Zeng, W., Liu, J., 2017. An end-to-end spatio-temporal attention model for human action recognition from skeleton data, in: *Thirty-first AAAI conference on artificial intelligence*.
- Sultani, W., Chen, C., Shah, M., 2018. Real-world anomaly detection in surveillance videos, in: *Proceedings of the IEEE Conference on Computer Vision and Pattern Recognition*, pp. 6479–6488.
- Suykens, J.A., Vandewalle, J., 1999. Least squares support vector machine classifiers. *Neural processing letters* 9, 293–300.
- Tajbakhsh, N., Gurudu, S.R., Liang, J., 2015. Automatic polyp detection in colonoscopy videos using an ensemble of convolutional neural networks, in: *Biomedical Imaging (ISBI), 2015 IEEE 12th International Symposium on*, IEEE. pp. 79–83.
- Tran, D., Bourdev, L., Fergus, R., Torresani, L., Paluri, M., 2015. Learning spatiotemporal features with 3d convolutional networks. *Proceedings of the IEEE International Conference on Computer Vision* , 4489–4497.
- Vaswani, A., Shazeer, N., Parmar, N., Uszkoreit, J., Jones, L., Gomez, A.N., Kaiser, Ł., Polosukhin, I., 2017. Attention is all you need, in: *Advances in Neural Information Processing Systems*, pp. 5998–6008.
- Wang, S., Cong, Y., Fan, H., Liu, L., Li, X., Yang, Y., Tang, Y., Zhao, H., Yu, H., 2016. Computer-aided endoscopic diagnosis without human-specific labeling. *IEEE Trans. on Bio Eng* 63, 2347–2358.
- Wang, X., Yan, Y., Tang, P., Bai, X., Liu, W., 2018. Revisiting multiple instance neural networks. *Pattern Recognition* 74, 15–24.
- Wei, D., Lim, J.J., Zisserman, A., Freeman, W.T., 2018. Learning and using the arrow of time, in: *Proceedings of the IEEE Conference on Computer Vision and Pattern Recognition*, pp. 8052–8060.
- Wu, J., Yu, Y., Huang, C., Yu, K., 2015. Deep multiple instance learning for image classification and auto-annotation, in: *Proceedings of the IEEE Conference on Computer Vision and Pattern Recognition*, pp. 3460–3469.
- Xu, K., Ba, J., Kiros, R., Cho, K., Courville, A., Salakhutdinov, R., Zemel, R., Bengio, Y., 2015. Show, attend and tell: Neural image caption generation with visual attention, in: *International conference on machine learning*, pp. 2048–2057.
- Zhou, Z.H., Xu, J.M., 2007. On the relation between multi-instance learning and semi-supervised learning, in: *Proceedings of the 24th international conference on Machine learning*, ACM. pp. 1167–1174.

Appendix A. Training Details:

Table A.4: Training configuration for all deep learning based methods when applicable

Configuration	Description
Input video (Bag) size	$30 \times 224 \times 224 \times 3$
Batch size	1
ResNet50 output feature size	2048
Number of Hidden Bidirectional LSTM	2
Hidden Bidirectional LSTM size	512
Detection threshold	0.5

Table A.5: Optimization procedure details

Experiment	Optimizer	Coef. β	Learning rate	Weight decay	Epochs	Stopping criteria
All	Adam	$\beta = (0.9, 0.999)$	(0.0001)Cyclic learning rate	0.0001	500	lowest validation error

Table A.6: MissSVM (Zhou and Xu (2007)) configuration

Method	Kernel	Regularization	Max-iteration
MissSVM	RBF	1	100

Table A.7: SIL (Ray and Craven (2005)) configuration

Method	Kernel	Regularization	Scale
SIL (Ray and Craven (2005))	Linear	10	False

Listing 1: PS-DeVCEM: Network configuration

```

1 ResNet50
2 AvgPool2d(kernel_size=7, stride=1, padding=0)
3 (lstm): LSTM(2048, 512, num_layers=2, bidirectional=True)
4 attention:
5 (0): Linear(in_features=1024, out_features=256, bias=True)
6 (1): Tanh()
7 (2): Linear(in_features=256, out_features=1, bias=True)
8 classifier:
9 (0): Linear(in_features=1024, out_features=15, bias=True)
10 (1): Sigmoid()
11 bagclassifier:
12 (0): Linear(in_features=1024, out_features=1, bias=True)
13 (1): Sigmoid()

```



(a) sup1.avi (Attached video):

(b) sup2.avi (Attached video):

(c) sup3.avi (Attached video):

Fig. A.10: We have attached sample videos with original video segment on the left side. The right side video shows the attention output. Dark frames represent low attention and original frame represents high attention value. The attention values are shown at the top. Fig. (A.10a) shows a video with multiple Diverticulosis on different frames. In this case, our method is able to localize the disease from the video labels. Fig. (A.10b) depicts Erosion and Erythema. Although the prediction for the video is correct, the network attention did not span all the frames with the diseases. Fig. (A.10c), the segment shows Tumor and Bleeding. As the video shows the Bleeding is not detected with our method. However, some part of the segment containing tumor were localized.